

Identification of an mtDNA Mutation Hot Spot in UV-Induced Mouse Skin Tumors Producing Altered Cellular Biochemistry

Jana Jandova^{1,3}, Alex Eshaghian^{2,3}, Mingjian Shi^{2,3}, Meiling Li², Lloyd E. King², Jaroslav Janda¹ and James E. Sligh¹

There is increasing awareness of the role of mtDNA alterations in the development of cancer, as mtDNA point mutations are found at high frequency in a variety of human tumors. To determine the biological effects of mtDNA mutations in UV-induced skin tumors, hairless mice were irradiated to produce tumors, and the tumor mtDNAs were screened for single-nucleotide changes using temperature gradient capillary electrophoresis (TGCE), followed by direct sequencing. A mutation hot spot (9821insA) in the *mitochondrially encoded tRNA arginine (mt-Tr)* locus (tRNA^{Arg}) was discovered in approximately one-third of premalignant and malignant skin tumors. To determine the functional relevance of this particular mutation *in vitro*, cybrid cell lines containing different *mt-Tr* (tRNA^{Arg}) alleles were generated. The resulting cybrid cell lines contained the same nuclear genotype and differed only in their mtDNAs. The biochemical analysis of the cybrids revealed that the mutant haplotype is associated with diminished levels of complex I protein (CI), resulting in lower levels of baseline oxygen consumption and lower cellular adenosine triphosphate (ATP) production. We hypothesize that this specific mtDNA mutation alters cellular biochemistry, supporting the development of keratinocyte neoplasia.

Journal of Investigative Dermatology advance online publication, 20 October 2011; doi:10.1038/jid.2011.320

INTRODUCTION

Theories of mitochondrial involvement on cancer date back to Warburg's theories that impairment of oxidative phosphorylation (OXPHOS) and increased use of glycolysis in tumors were thought to be critical steps in the development of cancer (Warburg, 1956). There is growing evidence that some nuclear-encoded OXPHOS genes have dual functions in energy generation and tumor suppression (Eng *et al.*, 2003). Mutations in the fumarate hydratase gene have been linked to uterine leiomyomas and renal cell carcinomas, and mutations in subunits of the succinate dehydrogenase gene (*SDHB*, *SHDC*, and *SDHD*) have been associated with paragangliomas, pheochromocytomas, and renal cell carcinomas (Baysal *et al.*, 2000; Niemann and Muller, 2000; Astuti *et al.*,

2001; Lehtonen *et al.*, 2004; Vanharanta *et al.*, 2004). The role of mtDNA point mutations in the development of cancer has been suggested (Polyak *et al.*, 1998; Petros *et al.*, 2005), as they have been found in high frequency in tumors. These mtDNA mutations were often homoplasmic (the exclusive mtDNA species), implying a genetic selection for these mtDNA changes in the development of cancers. mtDNA mutations have been identified in epithelial tumors, tumors of the musculoskeletal, central nervous, and endocrine systems (Brandon *et al.*, 2006; Chatterjee *et al.*, 2006; Lu *et al.*, 2009; Verma and Kumar, 2007).

mtDNA mutations have been studied in human skin cancer (Birch-Machin *et al.*, 1998; Berneburg *et al.*, 2006; Birch-Machin, 2006; Eshaghian *et al.*, 2006). One of the limitations in the analysis of mtDNA changes in humans is that they have many mtDNA polymorphisms that represent diverse cultural origins. The hairless mouse model system is useful for analysis of mtDNA changes in nonmelanoma skin cancer, as this model is a well-established way to generate epidermal tumors that are similar to those seen in human squamous cell carcinoma and the mtDNA is similar in size and structure to that of humans. Studying mtDNA changes in the laboratory mouse offers a distinct advantage of mtDNA homogeneity, which arises from a recent common female ancestor, and allows for a facilitated analysis of what mtDNA changes may be pathogenic (Ferris *et al.*, 1983). To determine whether mtDNA changes have a role in nonmelanoma skin cancer formation, tumors were induced in hairless mice by

¹Department of Medicine, Dermatology Division, Arizona Cancer Center, University of Arizona and the Southern Arizona VA Healthcare System, Tucson, Arizona, USA and ²VA Tennessee Valley Healthcare System, Dermatology Division of the Department of Medicine, and Department of Cell and Developmental Biology, Vanderbilt University Medical Center, Nashville, Tennessee, USA

³These authors contributed equally to this work.

Correspondence: James E. Sligh, Division of Dermatology, University of Arizona, 1515 North Campbell Avenue, Tucson, Arizona 85724, USA. E-mail: jsligh@azcc.arizona.edu

Abbreviations: ATP, adenosine triphosphate; CI, I, II, III, IV, V, mitochondrial complexes I, II, III, IV, V; mt-Tr, mitochondrially encoded tRNA arginine; OXPHOS, oxidative phosphorylation; ROS, reactive oxygen species; TGCE, temperature gradient capillary electrophoresis; tRNA, transfer RNA

Received 17 July 2011; accepted 11 August 2011

UV radiation. The DNA of these tumors was analyzed for mtDNA changes. A specific mutation in the *mitochondrially encoded tRNA arginine (mt-Tr)* locus occurred at high frequency, and this mutation was studied in a cybrid system to identify the specific biochemical changes imparted by the mtDNA mutation that are supportive of a tumorigenic phenotype.

RESULTS

To determine whether mtDNA changes occur in murine nonmelanoma skin cancers, tumors were induced in hairless SKH1 mice by UV irradiation (Figure 1a and b). The entire mouse mtDNA was screened for mutations using genomic DNA isolation from tumors, multiplexed PCR of the entire mtDNA, restriction endonuclease digestion (Figure 2a), and heteroduplex analysis by multiplexed temperature gradient capillary electrophoresis (TGCE; Figure 2b and c). A mutation hot spot was identified in the gene encoding the mitochondrial tRNA for arginine (*mt-Tr*). The presence of an additional peak for fragment 2 (arrow in Figure 2b) is indicative of a heteroduplex formation and the detection of a somatic mutation. Minimally irradiated skin from the ventral surface of each mouse was used as a control and was found to contain only homoduplexes, indicating the lack of any mutation. A 9821insA mutation in the *mt-Tr* locus was defined by DNA sequencing (Figure 2d-f). This mutation predicts an insertion of an extra A in a homopolymeric tract in the dihydrouridine loop of the mitochondrial tRNA^{Arg}. The B6 *mt-Tr* gene contains a homopolymeric tract of eight consecutive adenosine residues (Figure 2d). Tumors often contained an additional adenosine residue in this

tract (Figure 2e). This change was confirmed by re-amplifying and sequencing the gene in the reverse orientation, as well as by sequencing with *Pfu* DNA polymerase. This mutation was commonly seen in both heteroplasmy (Figure 2f) and homoplasmy (Figure 2e). The *mt-Tr* 9821insA mutation was found in approximately one-third of pre-malignant and malignant samples; however, it was absent in normal skin and other nontumor internal organs. The alleles present in the tumors include both heteroplasmic and homoplasmic 9821insA containing nine consecutive A bases instead of the eight that are normally found in this strain. Figure 1c shows the frequency of mutant *mt-Tr* 9821insA alleles in SKH1 mice that were irradiated with UV to induce cutaneous tumors. The “no tumor” skin is normal skin taken from the belly at the time of excision. “Other tissues” are healthy brain, liver, spleen, heart, kidney, and lung tissues taken from the same mice at the time of harvesting the skin tissues.

Structural analysis modeled with mfold software (Zuker, 2003) predicts the murine *mt-Tr* 9821insA allele containing nine adenosine residues to have potential altered secondary structures (Figure 3b and c). One of these structures is predicted to be similar to the *mt-Tr* wild-type allele containing eight consecutive adenosine residues (Figure 3a), whereas the other structure (Figure 3c) is markedly different and energetically more stable ($\Delta G = -11.3 \text{ kcal mol}^{-1}$) than the former structure ($\Delta G = -9.8 \text{ kcal mol}^{-1}$). As the transfer RNA (tRNA) structure is critical to its function, it is proposed that this altered structure would be more abundant and unlikely to be functional. At temperatures slightly lower than 37 °C, as are encountered in the skin, nonfunctional isoforms may be even more energetically favored over the typical wild-type allele structure. Thus, it is expected that cells containing *mt-Tr* 9821insA mutation allele would have affected protein synthesis of all 13 mtDNA-encoded peptides.

We used a naturally occurring allelic variant contained within the Balb/c mouse strain as the source of 9821insA allele. To determine the functional relevance of this single-nucleotide mutation, cybrid cells were generated. We produced two cybrid cell lines that had identical nuclear background to murine L cells but differed only in their mtDNA. In this way, the two alleles could be compared on a neutral nuclear genetic background. We analyzed the effects of this nucleotide insertion in the mtDNA by studying cybrids that harbor alterations at this locus.

We characterized the biochemistry of the cybrid cells by first examining cellular adenosine triphosphate (ATP) levels. Figure 4a shows that the cellular ATP levels were significantly lower in mtBALB cybrids compared with mtB6 cybrids in media containing glucose or galactose. Next, we examined respiratory activity of the cybrid lines by measuring cellular oxygen consumption. We observed that mtBALB cybrids consumed less oxygen compared with mtB6 cybrid cells overall under the basal conditions. After rotenone was added to inhibit CI, digitonin was used to permeabilize the cells, and the activity of CII was measured after adding the substrates adenosine diphosphate and succinate. Although the baseline levels of respiration were reduced in the mtBALB

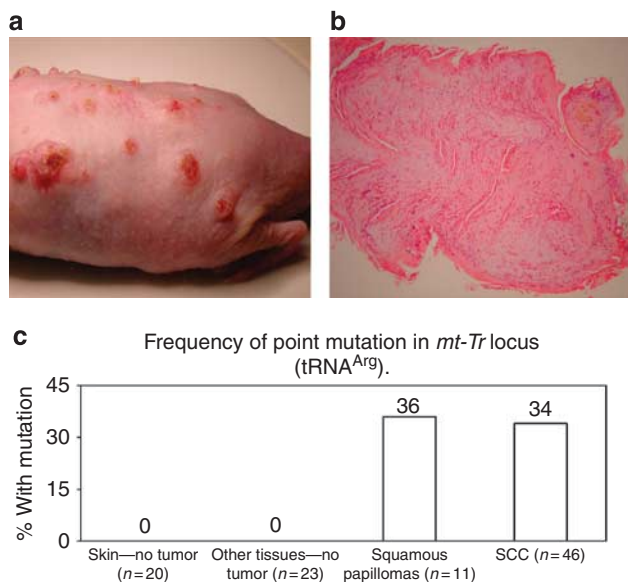


Figure 1. Induced cutaneous tumors and frequency of point mutation in the *mt-Tr* locus (tRNA^{Arg}). (a) Dorsal surface of a hairless mouse with UV-induced cutaneous tumors. (b) Hematoxylin and eosin histology stain of one of these tumors is consistent with a diagnosis of squamous papilloma. The height of the papilloma equals 2 mm. (c) The percentage of samples with various diagnoses harboring a mutant *mt-Tr* 9821insA allele is shown.

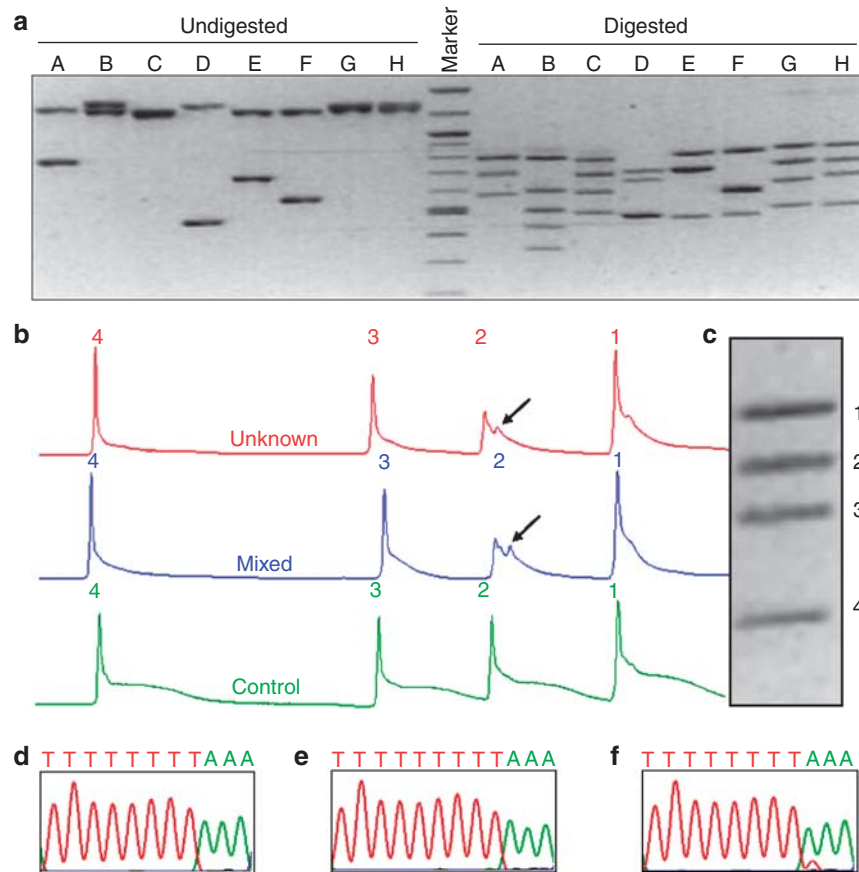


Figure 2. Restriction analysis, temperature gradient capillary electrophoresis (TGCE) multiplex analysis, and DNA sequencing detect mtDNA mutation hot spot. (a) Resolution of undigested PCR products covering the entire mtDNA (left) and digested restriction fragments (right) are shown in an inverted image of a 1.5% agarose gel stained with ethidium bromide. (b) TGCE output from a single capillary. Unknown (from a tumor, top), control (bottom), and mixed (center) mouse DNA samples were analyzed. Fragments 1, 3, and 4 have only a single peak, which is indicative of complete homoduplex formation and the lack of a mutation. The presence of an additional peak for fragment 2 in the unknown and mixed samples is indicative of heteroduplex formation and the detection of a somatic mutation. (c) The gel image of all four fragments. DNA sequencing of the *mt-Tr* locus in control and tumor DNA samples in reverse orientation. (d) Partial DNA sequence of wild-type allele and (e) homoplasmic or (f) heteroplasmic 9821insA mutant allele.

cybrids compared with mtB6, they displayed significantly enhanced oxygen consumption in the presence of CII substrates (Figure 4b). To better understand the observed changes in respiration, we sought to characterize the levels of OXPHOS proteins contained within the mitochondria. Using western blotting, we compared the protein levels of all mitochondrial OXPHOS complexes of mtB6 and mtBALB cybrid cells (Figure 5a). The levels of CI were significantly reduced in mtBALB cybrids compared with mtB6, as measured by densitometry. The levels of complexes II, III, IV, and V showed no significant differences between the cell lines (Figure 5b). Thus, mtBALB cybrids have a diminished overall respiratory activity compared with mtB6 cybrids, but they are more responsive to CII substrates.

DISCUSSION

The tumors generated in the mouse occurred primarily on the UV-exposed dorsal surfaces of the animals and were malignant squamous cell carcinomas or premalignant squamous

papillomas by microscopic analysis performed by a dermatopathologist. One particular point mutation in the *mt-Tr* locus (tRNA^{Arg}) was very common, occurring in approximately one-third of squamous papilloma samples and squamous cell carcinoma samples (Figure 1c); however, it was not detected in normal skin from the minimally irradiated ventral surface of animals or in normal-appearing skin from the irradiated dorsal surface of the animals, nor was it detected in internal organs, indicating that these induced changes occurred in the process of tumor development. The mouse mitochondrial *mt-Tr* (tRNA^{Arg}) gene appears to be a hot spot for UV-induced mutations having the sequence containing a homopolymeric tract of eight consecutive adenosine residues. The occurrence of an insertion mutation within a homopolymeric tract may highlight a potential weakness in the ability of mitochondrial DNA polymerase- γ to repair UVA-induced damage within the mtDNA (Longley *et al.*, 2001). Such mutations may be important in tumor progression, as mtDNA changes lead to increased oxidative

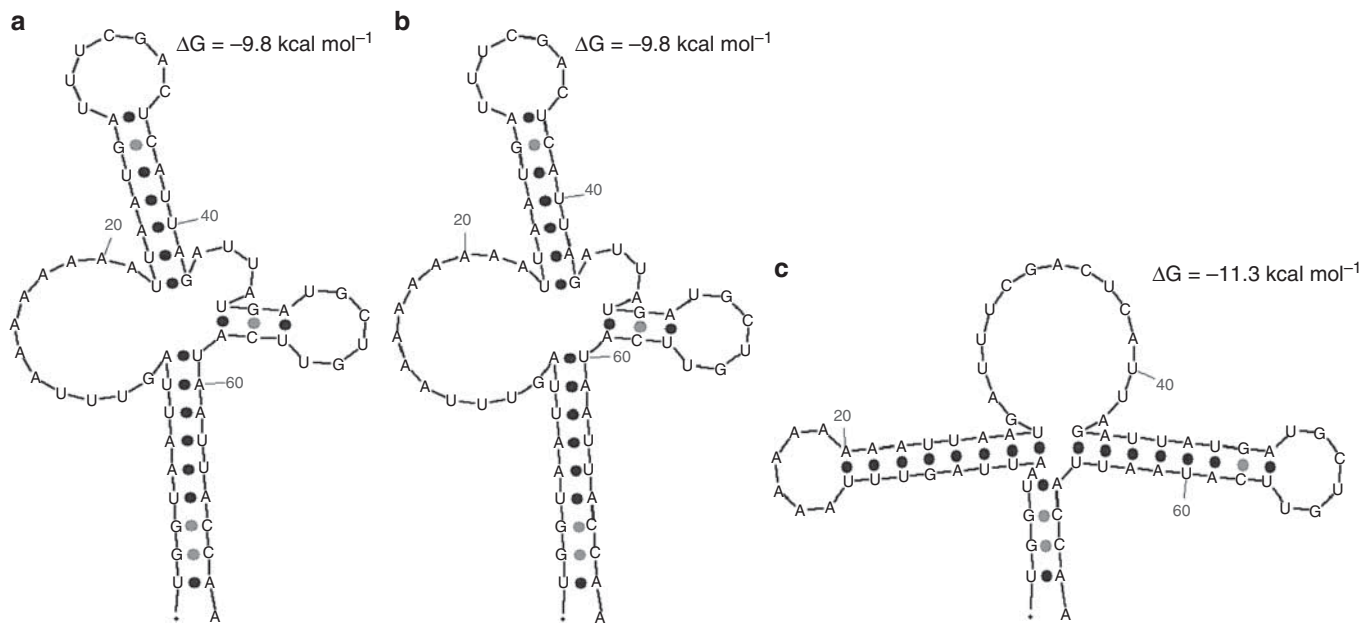


Figure 3. Predicted transfer RNA (tRNA) structures based on sequence. The predicted structures for the tRNA variants generated by mfold software. (a) Wild-type tRNA isoform with $\Delta G = -9.8 \text{ kcal mol}^{-1}$, (b) 9821insA tRNA isoform with $\Delta G = -9.8 \text{ kcal mol}^{-1}$, and (c) 9821insA tRNA isoform with $\Delta G = -11.3 \text{ kcal mol}^{-1}$.

stress, which can be mitogenic to cells (unpublished observations). We generated cybrid cell lines to identify biochemical and molecular changes because of this genetic alteration in the *mt-Tr* gene. As tRNAs are required for protein synthesis, the levels of all mtDNA-encoded polypeptides can be altered. The western blot analysis revealed that the mutant haplotype is associated with diminished levels of complex I protein, which is likely caused because a portion of the 9821insA tRNAs are nonfunctional. These decreased levels of complex I protein resulted in lower levels of baseline oxygen consumption and lower cellular ATP production. The mtBALB cybrids are more responsive to CII substrates. CII subunits are entirely encoded within the nuclear DNA and these proteins are synthesized on cytoplasmic ribosomes before import into the mitochondria. Enhanced CII substrate sensitivity may reflect a compensatory change by the nucleus to compensate for lower overall cellular ATP levels.

The biochemical differences between the cybrids suggest that energetic metabolism may be directly linked to neoplastic behavior. This notion of glycolytic metabolism as a key component of cellular transformation was proposed more than 50 years ago (Warburg, 1956). A recent study by Ye *et al.* (2011) reported that some mitochondrial and energy metabolism-related properties, such as lower oxygen/glucose consumption, and lower intracellular concentrations of ATP can be used as indicators of lung cancer stem cells. Much lower rates of ATP synthesis, lower cellular oxygen consumption, and decreased activities of the respiratory chain complexes were found in breast cancer cells (Ma *et al.*, 2010). Moreover, downregulation of the catalytic subunit of the mitochondrial ATP synthase has been found to be a hallmark of many types of cancer such as liver, kidney, colon, breast, lung, and squamous esophageal carcinomas and gastric

adenocarcinomas (Formentini *et al.*, 2010). Oncocytic tumors of the thyroid, kidney, and parathyroids have been shown to accumulate mtDNA disruptive mutations, the large majority of which map in respiratory CI genes (Costa-Guda *et al.*, 2007; Gasparre *et al.*, 2007, 2008, 2009; Mayr *et al.*, 2008; Zimmermann *et al.*, 2009; Porcelli *et al.*, 2010). In oncocytomas, a consistent loss of CI was found, along with compensatory upregulation of the other respiratory chain complexes (Zimmermann *et al.*, 2011). The involvement of CI mutations in cancer has been demonstrated in a recent study of sporadic breast cancer (Czarnecka *et al.*, 2010).

The oxidative damage generated by UV radiation may also increase the levels of reactive oxygen species (ROS) to the point where the cells begin to hyperproliferate and other carcinogenic phenotypes such as migration and invasiveness can be triggered. The measurement of proliferative and migratory changes may be valuable in explaining the higher incidence of this genetic change in tumors. In addition, the possible differences in ROS production between the two cybrid lines should be determined, as ROS levels can support a role of ROS as specific second messengers (Burdon, 1995; Irani *et al.*, 1997; Sauer *et al.*, 2001; Liu *et al.*, 2002; Nishikawa, 2008; Mesquita *et al.*, 2010) in signaling cascades involved in cell proliferation, differentiation, and migration.

Inheritance of these mtDNA changes at the *mt-Tr* locus in mice is associated with deafness (Johnson *et al.*, 2001), as well as with modulation of complex phenotypes such as cognitive functions (Roubertoux *et al.*, 2003). Different phenotypes associated with mtDNA variation at the same locus are common in human mtDNA-associated diseases in which tRNA mutations, in particular, often produce very pleomorphic phenotypes such as those seen in human tRNA^{Leu} gene (Wittenhagen and Kelley, 2003). The 9821insA allele may be

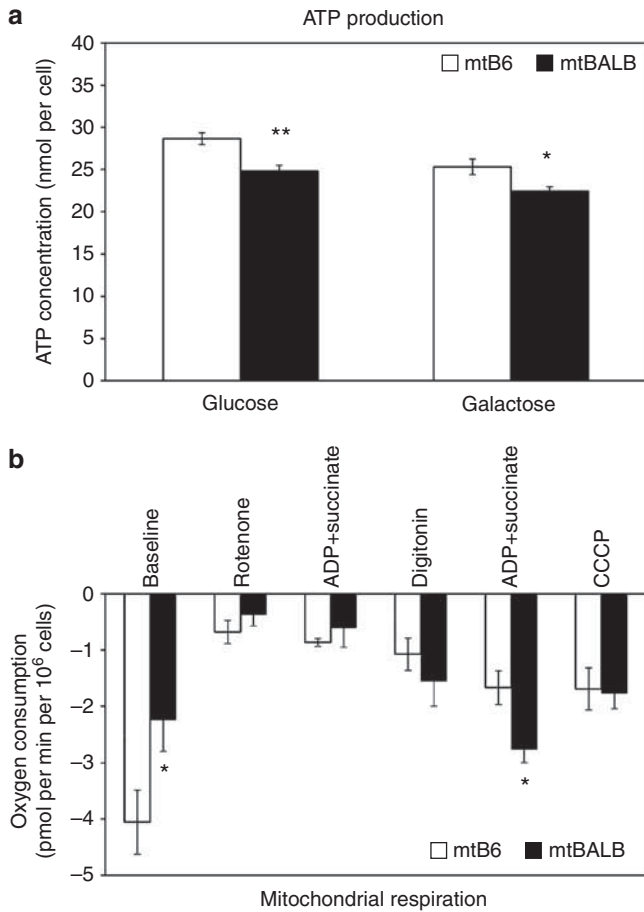


Figure 4. The mtBALB cybrid cells have lower adenosine triphosphate (ATP) production and altered respiratory function compared with mtB6 cybrids. (a) Cybrid cells were incubated in DMEM supplemented with either glucose or galactose. The levels of cellular ATP are shown. (b) Fiber optic investigation of mitochondrial respiratory chain function showing oxygen consumption was performed without the addition of an exogenous substrate, and with the addition of specific oxidative phosphorylation (OXPHOS) substrates or inhibitors. Values represent the mean \pm SEM of three independent experiments of five clones. CCCP, carbonyl cyanide *m*-chlorophenylhydrazone. Asterisks indicate statistical difference between mtB6 and mtBALB cybrid cells (* P <0.05, ** P <0.005).

expected to form different structurally distinct isoforms that may have a normal or possibly nonexistent function. The balance of functional to nonfunctional isoforms may be quite tissue specific, depending on local factors such as temperature or ionic concentrations. Homeostasis imbalance in the organism may predispose to organ-specific tumor development.

In this study we identify a hot spot for mutations and demonstrate that this *mt-Tr* 9821insA allele can alter the biochemical characteristics of murine cybrid cells. These profound differences in cellular physiology displayed by the murine cybrids may contribute to the overall tumorigenic phenotype of the tumors that harbor this mtDNA change and may also explain some of the varying predispositions to developing tissue-specific malignancies in mouse strains (Krupke *et al.*, 2008). Furthermore, these studies on mouse

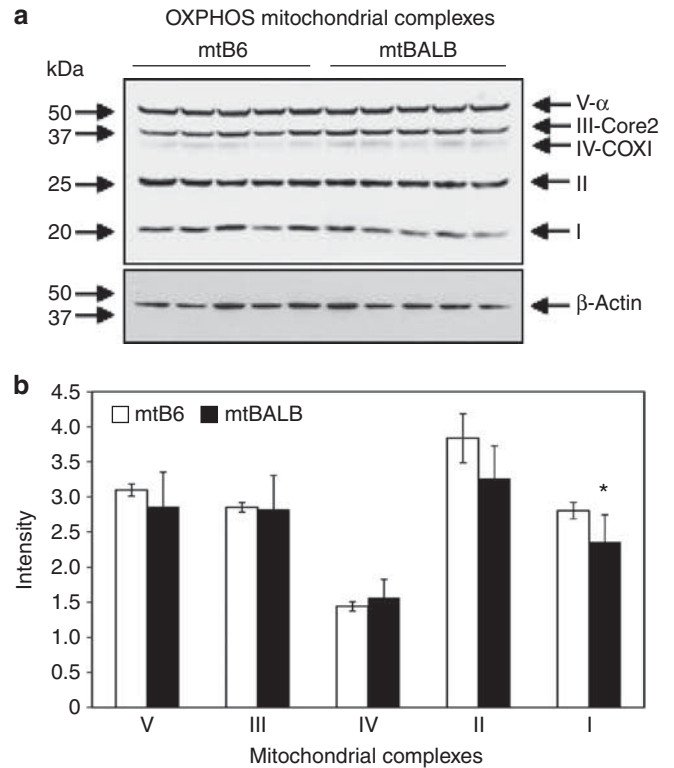


Figure 5. Complex I levels are lower in mtBALB cybrid cells compared with mtB6. (a) Five mouse monoclonal antibodies to mitochondrial oxidative phosphorylation (OXPHOS) subunits were used to detect protein levels by western blot analysis. (b) Densitometry of western blot analysis showing reduced levels of complex I protein. The level of complex I, II, III, IV, and V subunits is expressed as the relative intensity of the immunoblots normalized to β -actin loading control. Data are mean \pm SEM of three independent experiments of five clones. Asterisk indicates statistical difference between mtB6 and mtBALB cybrid cells (* P <0.05).

mtDNA haplotypes contribute to a better understanding of human phenotypes associated with mtDNA variation.

MATERIALS AND METHODS

Mice

To study hairless mice with the mitochondrial background of C57BL/6J (B6), SKH1 hairless male mice (Charles River Laboratories, Wilmington, MA) were crossed with female B6 mice (The Jackson Laboratory, Bar Harbor, ME) and the resulting female progenies were backcrossed 10 times with SKH1. Female F2 mice that were hairless and albino were selected from each cross for continued backcrossing with SKH1 male mice. BALB/cj mice (The Jackson Laboratory) have mtDNA identical to B6 mice. The only differences between their mtDNAs are a T to C polymorphism at 9461 and a 9348 G to A change resulting in the amino acid change V248I, which is thought to be a neutral polymorphism (Moreno-Loshuertos *et al.*, 2006) and an additional A insertion in the *mt-Tr* locus resulting in the expansion of a homopolymeric tract of eight consecutive A residues to nine consecutive A's in the pseudouridine loop of the tRNA^{Arg} molecule.

The animal experiments were approved by the institutional animal care and use committees at the Vanderbilt University and the University of Arizona.

Tumor induction

Cutaneous tumors were induced in hairless SKH1 mice by exposure to 720 mJ UVA and 60 mJ UVB 5 days per week for 10 weeks. Tumor formation began several weeks later. Tumors were removed from the dorsal surface of the animals, along with minimally irradiated skin from the ventral surface of the animals, and in some cases tumor-free irradiated skin was removed from the dorsal surface of the animals, as a control. After killing, non-UV-irradiated tissues including brain, heart, skeletal muscle, gut, liver, spleen, gonads, and lungs were isolated. The mtDNA of these UV-protected organs was also used as controls. Genomic DNA was isolated from each tumor, and mtDNA was analyzed for single-nucleotide changes using TGCE.

Temperature Gradient Capillary Electrophoresis

DNA extraction was performed using DNeasy kits (Qiagen, Valencia, CA) or by alkaline lysis and protein precipitation after proteinase K tissue digestion.

The entire mouse mtDNA was PCR amplified in overlapping fragments in 8 tubes using 16 mtDNA-specific primer pairs (Table 1). Each tube contained two primer pairs, and two PCR products were produced per tube. Thirty cycles of multiplexed PCR were performed in Ampli-Taq Gold buffer (Applied Biosystems, Carlsbad, CA) with 15 mM MgCl₂, according to the manufacturer's instructions, supplemented with additional 25 mM MgCl₂, 2 mM dNTP (New England BioLabs, Ipswich, MA), 5 μM primers, 10 μg μl⁻¹ BSA (Promega), and 9:1 Ampli-Taq Gold/*Pfu* DNA polymerase (Promega). The PCR parameters were as follows: an initial denaturation at 95 °C for 10 minutes, followed by 30 cycles of denaturation at 95 °C for 1 minute, annealing at 57 °C for 1 minute, and elongation at 72 °C for 3 minutes, with a final elongation at 72 °C for 10 minutes.

Restriction endonuclease digestions of crude PCR products were performed in the augmented Ampli-Taq Gold buffer without further supplementation at 37 °C, except for *TaqI*, which was digested at 65 °C. A volume of 2 μl of the appropriate restriction enzyme (Table 1) was added to every PCR product. Samples were incubated at 37 °C for 2 hours and then at 65 °C for 60 minutes. To determine the resolution of all restriction fragments, 5 μl of restriction fragments from each tube was run on 1.5% agarose gel electrophoresis at 10 V cm⁻¹ for 90 minutes.

Heteroduplex species are formed by mixing digested unknown DNA fragments with control DNA fragments in a 1:1 ratio in a thermal cycler. The mixed samples are denatured at 95 °C and annealed using this profile: a 3-minute denaturation step at 95 °C, followed by a stepwise reduction in temperature as follows: decrease from 95 to 80 °C at 3 °C per minute, decrease from 80 to 55 °C at 1 °C per minute, hold for 20 minutes at 55 °C, decrease from 55 to 45 °C at 1 °C per minute, and decrease from 45 to 25 °C at 2 °C per minute before storage at 4 °C.

TGCE analysis was performed on a Reveal Discovery System (SpectruMedix, State College, PA). This system performs temperature gradient electrophoresis for DNA variant detection in an automated capillary array instrument. DNA samples consisting of homoduplexes and heteroduplexes are separated by capillary electrophoresis, during which a thermal ramp from 50 to 60 °C for 25 minutes is applied. The injection parameters are 6 kV for 90 seconds and the capillary length is 70 cm. The gel in the capillary is 2% w/v 7-million mol wt polyethylene oxide dissolved in 1 × TBE buffer with ethidium bromide added at a final concentration of

0.5 μg ml⁻¹. SpectruMedix Check Mate Software was used for instrument control and data acquisition (acquisition time 65 minutes). Data were analyzed using SpectruMedix Reveal Software to generate mutation scoring results for all samples in a plate.

DNA sequencing

Forward (5'-TTCTAGTCACAATTCTATCTCTAGGC-3') and reverse (5'-GCATTGTAGTAGGTTGAGATTTTGG-3') primers were designed for PCR to amplify the *mt-Tr* gene from total genomic DNA. PCR samples were prepared in a total volume of 50 μl. Each tube contained 1 × Taq master Mix (New England BioLabs) containing 10 mM Tris-HCl, 50 mM KCl, 1.5 mM MgCl₂, 25 units ml⁻¹ Taq DNA polymerase, 0.2 mM dNTPs each, 5% glycerol, 0.08% NP-40, and 0.05% Tween-20, as well as 250 ng of DNA template and 5 μM of both primers. The PCR parameters were as follows: an initial denaturation at 95 °C for 5 minutes, followed by 30 cycles of denaturation at 95 °C for 30 seconds, annealing at 60 °C for 60 seconds, and elongation at 68 °C for 1 minute, with a final elongation at 68 °C for 5 minutes. PCR products were then purified using the QIAquick PCR purification kit (Qiagen) and sequenced on an Applied Biosystems 3730XL DNA analyzer (Life Technologies, Carlsbad, CA).

Cybrid cell line generation

LMEB3(mtBALB) and LMEB3(mtB6) cells were generated by harvesting mitochondria from brain synaptosomes of B6 and BALB mice and electrofusing them to a mouse fibroblast LMEB3p⁰ cell line that lacked its own mtDNA (Trounce and Wallace, 1996; Trounce *et al.*, 2000). All cell lines were grown in high glucose (4.5 g l⁻¹) or in galactose (4.5 g l⁻¹) DMEM (Invitrogen, Carlsbad, CA) supplemented with 10% fetal bovine serum (Invitrogen, Carlsbad, CA) as indicated.

ATP assay

The amount of cellular ATP was determined using an ATPlite 1step kit (PerkinElmer, Waltham, MA) based on firefly luciferin/luciferase (Cree and Andreotti, 1997). Cells were seeded in 96-well plates (5 × 10⁴ per well) and allowed to attach for 4 hours. They were then washed with Dulbecco's phosphate-buffered saline and incubated in DMEM (Invitrogen) with glucose or galactose for 16 hours. The plates were removed from the incubator and allowed to equilibrate at room temperature for 30 minutes. Next, 100 μl of ATPlite 1step reagent was added to each well and the plates were shaken for 10 minutes at 700 r.p.m. using a rotary plate shaker. The measurements of mitochondrial ATP levels were taken using a Veritas luminometric plate reader (Turner Biosystems, Madison, WI). The ATP levels were expressed as nmoles per cell.

Respiration assay

Oxygen consumption rates were measured in whole cells by using a Fiber optic oxygen monitor (Instech Laboratories, Plymouth Meeting, PA). Briefly, cells were suspended in 1 ml of respiratory buffer (10 mM Hepes, pH 7.4, 225 mM mannitol, 75 mM sucrose, 10 mM KCl, 10 mM KH₂PO₄, 5 mM MgCl₂, and 1 mg ml⁻¹ BSA) at a concentration of 2 × 10⁶ cells per ml at 37 °C in a magnetically stirred 1.2 ml chamber. The decrease in O₂ concentration in the sealed chamber was measured as cellular oxygen consumption by an O₂ fiber optic sensor. Baseline respiration was recorded for 2 minutes before 2 μl aliquots of 0.1 mM rotenone (Sigma Aldrich, St Louis, MO) were added until total inhibition of complex I was obtained. Cell membrane integrity was

Table 1. Overview of multiplex system for mouse mtDNA genome sequencing

Tube ID	Start	End	Size	Forward primer (5' to 3')	Reverse primer (5' to 3')	Restriction enzyme	Restriction fragment
A1	1,050	2,340	1,291	TCTGGCCTACCCAGAAAGATTCA	CTGGGTCAATAAGATATGTTGATTTACTTTGACT	<i>EcoRI</i>	759,700,591
A2	8,465	9,223	759	TATTAATAAATATTAGCCACCAACAGCTACCATT	AGTCCATGGAATCCAGTAGCCATGA		
B1	7,168	8,461	1,294	TACAAGCACAAATAGATGCACAAGAAGTTGA	GAGTAGCTCCTCCGATTAGGTGTTAATAAAGTGT	<i>TaqI</i>	794,597,500,431,338
B2	14,915	16,280	1,365	TAATCCACTAAACACCCACCCCATATT	GCGTAATAGAGTATGATTAGAGTTTTGGTTCACG		
C1	11,399	12,666	1,267	CACCCAACGCGGCAAACAACTAAC	CTAGTTGGCTTGATGTAGAGAAGGCAATG	<i>TaqI</i>	770,681,587,487
C2	16,159	1,121	1,257	TCAAACCCTATGTCCTGATCAATTCTAGTAGTTC	TTTGTGTAGGGCTAGGGCTAGGATTAGTT		
D1	5,828	6,299	472	TATTATCAACATGAAACCCAGCCATA	AAGTCAGCTAAATCTTTGACACCGGTAGG	<i>DraI</i>	694,595,472
D2	9,220	10,508	1,289	GACTCCATGTAATTATTGGATCAACATTCCT	AATTAGTTCAGTTGCTGAAAAGGTTATGATTAGG		
E1	2,248	3,507	1,260	GGTGGGGTGACCTCGGAGAAT	CTGGTAAATTGATATAGTATAGGGGCTCAGGAAGA	<i>DraI</i>	793,701,467
E2	6,550	7,250	701	CATGAGCAAAAAGCCACTTCG	AGGGGAGAGCAATTATGATAAGGATTACAGC		
F1	6,123	6,700	578	GAACCTTCGGCTATATAGGAATAGTATGAGCAAT	GATCCTATAGAAGAGACAGTGTTCATGTGGTG	<i>DraI</i>	801,578,468
F2	13,701	14,969	1,269	CTCCCAAACATCAAGATTAATTACTCCAA	TGCAAATAGGAAATATCATTCCGGTTTAAT		
G1	4,661	5,988	1,328	TCCCTAGGAGGCCTCCACCAC	CAAAGAAAGTTGTGTTAGGTTGCCGTCT	<i>DraI</i>	809,715,613,501
G2	10,194	11,503	1,310	CTACCCTAACCTGACTATCAAGCCCTAAAA	GTTAGAAGAATAAGTGAATTATGTGAAGGGCTAT		
H1	3,407	4,700	1,294	ATTCGCGTTATCTTTATAGCAGAGTACACTAACA	TTGGTAAGAATCCTGTTAGTGGTGAAG	<i>DraI</i>	807,703,633,487
H2	12,487	13,822	1,336	CAATAGTAGTTCAGGAATTTCTACTGCTC	TTGGGGATCTAACTGATTAATTTGGGTTT		

Eight tubes (A–H) per sample were used to amplify the entire murine mitochondrial genome. Two PCR products (1 and 2) were generated in each tube. These pairs of PCR products were subsequently digested with various restriction enzymes to generate restriction fragments and single-nucleotide changes were detected using temperature gradient capillary electrophoresis (TGCE). The start, end, and size of each PCR product is listed along with the primers used to generate the PCR products, the restriction enzymes used, and the sizes of the fragments generated via the restriction enzymes.

controlled by measuring succinate-driven respiration (10 µl of 0.1 M adenosine diphosphate plus 20 µl of 1 M succinate, pH 7.4) before and after digitonin permeabilization. Cells were permeabilized using 2 µl of 5 mg ml⁻¹ digitonin (Sigma Aldrich) per 1 × 10⁶ cells. Maximum uncoupled respiration rate was obtained by the addition of 2 µl of 2.5 mM carbonyl cyanide *m*-chlorophenylhydrazone (data not shown). Finally, inhibited respiration was measured after the addition of 2 µl of 200 mM potassium cyanide (data not shown).

Western blotting analysis of OXPHOS complexes

Cybrid cells were collected and resuspended in RIPA buffer (50 mM Tris-HCl, pH 7.4, 150 mM NaCl, 1 mM PMSF, 1 mM EDTA, 5 µg ml⁻¹ Aprotinin, 5 µg ml⁻¹ Leupeptin, 1% Triton X-100, 1% Sodium deoxycholate, and 0.1% SDS; Sigma Aldrich). Protein content was assessed by Coomassie staining. Protein (20 µg) was separated by 12% SDS-PAGE electrophoresis and transferred onto a nitrocellulose membrane (Bio-Rad, Hercules, CA). MitoProfile Total OXPHOS Rodent WB Antibody Cocktail (MitoSciences, Eugene, OR) containing five monoclonal antibodies against the 20 kDa subunit of complex I, ND6, CII-30 kDa, CIII-Core protein 2, CIV subunit I, and CV-α subunit, was used to detect complex I–V subunits, respectively. The membrane was stripped and re-blotted with rabbit β-actin mAb (Cell Signaling Technology, Danvers, MA) to normalize protein-loading levels. Dilutions of different antibodies for immunoblotting and subsequent detection by the enhanced chemiluminescence ECL plus system (GE Healthcare Biosciences, Pittsburgh, PA) were carried out according to the manufacturer's protocol.

Statistical analysis

Data are represented as mean ± SEM of five clones. All experiments were performed at least three times. Statistical significance between any two groups was determined using the two-tailed Student's *t*-test. The *P*-values of <0.05 were considered to be significant.

CONFLICT OF INTEREST

The authors state no conflict of interest.

ACKNOWLEDGMENTS

This work was supported by NCI Cancer Center Support grant P30 CA023074 (CCSG) and R01 AR 0501552 to JES, by the VA Advanced Career Development Award and VA Merit Award to JES, and by the Vanderbilt Skin Diseases Research Center Core grant (NIH P30AR41943).

REFERENCES

- Astuti D, Latif F, Dallol A *et al.* (2001) Gene mutations in the succinate dehydrogenase subunit SDHB cause susceptibility to familial pheochromocytoma and to familial paraganglioma. *Am J Hum Genet* 69: 49–54
- Baysal BE, Ferrell RE, Willett-Brozick JE *et al.* (2000) Mutations in SDHD, a mitochondrial complex II gene, in hereditary paraganglioma. *Science* 287:848–51
- Berneburg M, Kamenisch Y, Krutmann J *et al.* (2006) 'To repair or not to repair - no longer a question': repair of mitochondrial DNA shielding against age and cancer. *Exp Dermatol* 15:1005–15
- Birch-Machin MA (2006) The role of mitochondria in ageing and carcinogenesis. *Clin Exp Dermatol* 31:548–52

- Birch-Machin MA, Tindall M, Turner R *et al.* (1998) Mitochondrial DNA deletions in human skin reflect photo- rather than chronologic aging. *J Invest Dermatol* 110:149–52
- Brandon M, Baldi P, Wallace DC (2006) Mitochondrial mutations in cancer. *Oncogene* 25:4647–62 (abstract)
- Burdon RH (1995) Superoxide and hydrogen-peroxide in relation to mammalian-cell proliferation. *Free Radical Bio Med* 18:775–94
- Chatterjee A, Mambo E, Sidransky D (2006) Mitochondrial DNA mutations in human cancer. *Oncogene* 25:4663–74
- Costa-Guda J, Tokura T, Roth SI *et al.* (2007) Mitochondrial DNA mutations in oxyphilic and chief cell parathyroid adenomas. *BMC Endocr Disord* 7:8
- Cree IA, Andreotti PE (1997) Measurement of cytotoxicity by ATP-based luminescence assay in primary cell cultures and cell lines. *Toxicol in Vitro* 11:553–6
- Czarnecka AM, Krawczyk T, Zdrozny M *et al.* (2010) Mitochondrial NADH-dehydrogenase subunit 3 (ND3) polymorphism (A10398G) and sporadic breast cancer in Poland. *Breast Cancer Res Treat* 121:511–8
- Eng C, Kiuru M, Fernandez MJ *et al.* (2003) A role for mitochondrial enzymes in inherited neoplasia and beyond. *Nat Rev Cancer* 3:193–202
- Eshaghian A, Vleugels RA, Canter JA *et al.* (2006) Mitochondrial DNA deletions serve as biomarkers of aging in the skin, but are typically absent in nonmelanoma skin cancers. *J Invest Dermatol* 126:336–44
- Ferris SD, Sage RD, Prager EM *et al.* (1983) Mitochondrial-DNA evolution in mice. *Genetics* 105:681–721
- Formentini L, Martínez-Reyes I, Cuezva JM (2010) The mitochondrial bioenergetic capacity of carcinomas. *IUBMB Life* 62:554–60
- Gasparre G, Hervouet E, de Laplanche E *et al.* (2008) Clonal expansion of mutated mitochondrial DNA is associated with tumor formation and complex I deficiency in the benign renal oncocytoma. *Hum Mol Genet* 17:986–95
- Gasparre G, Iommarini L, Porcelli AM *et al.* (2009) An inherited mitochondrial DNA disruptive mutation shifts to homoplasmy in oncocytic tumor cells. *Hum Mutat* 30:391–6
- Gasparre G, Porcelli AM, Bonora E *et al.* (2007) Disruptive mitochondrial DNA mutations in complex I subunits are markers of oncocytic phenotype in thyroid tumors. *Proc Natl Acad Sci USA* 104:9001–6
- Irani K, Xia Y, Zweier JL *et al.* (1997) Mitogenic signaling mediated by oxidants in ras-transformed fibroblasts. *Science* 275:1649–52
- Johnson KR, Zheng QY, Bykhovskaya Y *et al.* (2001) A nuclear-mitochondrial DNA interaction affecting hearing impairment in mice. *Nat Genet* 27:191–4
- Krupke DM, Begley DA, Sundberg JP *et al.* (2008) The mouse tumor biology database. *Nat Rev Cancer* 8:459–65
- Lehtonen R, Kiuru M, Vanharanta S *et al.* (2004) Biallelic inactivation of fumarate hydratase (FH) occurs in nonsyndromic uterine leiomyomas but is rare in other tumors. *Am J Pathol* 164:17–22
- Liu SL, Lin X, Shi DY *et al.* (2002) Reactive oxygen species stimulated human hepatoma cell proliferation via cross-talk between PI3-K/PKB and JNK signaling pathways. *Arch Biochem Biophys* 406:173–82
- Longley MJ, Nguyen D, Kunkel TA *et al.* (2001) The fidelity of human DNA polymerase γ with and without exonucleolytic proofreading and the p55 accessory subunit. *J Biol Chem* 276:38555–62
- Lu J, Sharma LK, Bai Y (2009) Implications of mitochondrial DNA mutations and mitochondrial dysfunction in tumorigenesis. *Cell Res* 19:802–15 (abstr.)
- Ma Y, Bai RK, Trieu R *et al.* (2010) Mitochondrial dysfunction in human breast cancer cells and their transmitochondrial cybrids. *Biochim Biophys Acta* 1797:29–37
- Mayr JA, Meierhofer D, Zimmermann F *et al.* (2008) Loss of complex I due to mitochondrial DNA mutations in renal oncocytoma. *Clin Cancer Res* 14:2270–5
- Mesquita FS, Dyer SN, Heinrich DA *et al.* (2010) Reactive oxygen species mediate mitogenic growth factor signaling pathways in human leiomyoma smooth muscle cells. *Biol Reprod* 82:341–51
- Moreno-Loshuertos R, Acin-Perez R, Fernandez-Silva P *et al.* (2006) Differences in reactive oxygen species production explain the phenotypes associated with common mouse mitochondrial DNA variants. *Nat Genet* 38:1261–8
- Niemann S, Muller U (2000) Mutations in SDHC cause autosomal dominant paraganglioma, type 3. *Nat Genet* 26:268–70
- Nishikawa M (2008) Reactive oxygen species in tumor metastasis. *Cancer Lett* 266:53–9
- Petros JA, Baumann AK, Ruiz-Pesini E *et al.* (2005) mtDNA mutations increase tumorigenicity in prostate cancer. *Proc Natl Acad Sci USA* 102:719–24
- Polyak K, Li Y, Zhu H *et al.* (1998) Somatic mutations of the mitochondrial genome in human colorectal tumours. *Nat Genet* 20:291–3
- Porcelli AM, Ghelli A, Ceccarelli C *et al.* (2010) The genetic and metabolic signature of oncocytic transformation implicates HIF1 α destabilization. *Hum Mol Genet* 19:1019–32
- Roubertoux PL, Sluyter F, Carlier M *et al.* (2003) Mitochondrial DNA modifies cognition in interaction with the nuclear genome and age in mice. *Nat Genet* 35:65–9
- Sauer H, Wartenberg M, Hescheler J (2001) Reactive oxygen species as intracellular messengers during cell growth and differentiation. *Cell Physiol Biochem* 11:173–86
- Trounce I, Schmiedel J, Yen HC *et al.* (2000) Cloning of neuronal mtDNA variants in cultured cells by synaptosome fusion with mtDNA-less cells. *Nucleic Acids Res* 28:2164–70
- Trounce I, Wallace DC (1996) Production of transmitochondrial mouse cell lines by cybrid rescue of rhodamine-6G pre-treated L-cells. *Somat Cell Mol Genet* 22:81–5
- Vanharanta S, Buchta M, McWhinney SR *et al.* (2004) Early-onset renal cell carcinoma as a novel extraparaganglial component of SDHB-associated heritable paraganglioma. *Am J Hum Genet* 74:153–9
- Verma M, Kumar D (2007) Application of mitochondrial genome information in cancer epidemiology. *Clin Chim Acta* 383:41–50
- Warburg O (1956) Origin of cancer cells. *Science* 123:309–14
- Wittenhagen LM, Kelley SO (2003) Impact of disease-related mitochondrial mutations on tRNA structure and function. *Trends Biochem Sci* 28:605–11
- Ye XQ, Li Q, Wang GH *et al.* (2011) Mitochondrial and energy metabolism-related properties as novel indicators of lung cancer stem cells. *Int J Cancer* 129:820–31
- Zimmermann FA, Mayr JA, Feichtinger R *et al.* (2011) Respiratory chain complex I is a mitochondrial tumor suppressor of oncocytic tumors. *Front Biosci* 3:315–25
- Zimmermann FA, Mayr JA, Neureiter D *et al.* (2009) Lack of complex I is associated with oncocytic thyroid tumours. *Br J Cancer* 100:1434–7
- Zuker M (2003) Mfold web server for nucleic acid folding and hybridization prediction. *Nucleic Acids Res* 31:3406–15